



HAL
open science

Temperature-dependent viscoelastic modeling of ground deformation: Application to Etna volcano during the 1993-1997 inflation period

Ciro del Negro, Gilda Currenti, Danila Scandura

► To cite this version:

Ciro del Negro, Gilda Currenti, Danila Scandura. Temperature-dependent viscoelastic modeling of ground deformation: Application to Etna volcano during the 1993-1997 inflation period. *Physics of the Earth and Planetary Interiors*, 2008, 172 (3-4), pp.299. 10.1016/j.pepi.2008.10.019 . hal-00532184

HAL Id: hal-00532184

<https://hal.science/hal-00532184>

Submitted on 4 Nov 2010

HAL is a multi-disciplinary open access archive for the deposit and dissemination of scientific research documents, whether they are published or not. The documents may come from teaching and research institutions in France or abroad, or from public or private research centers.

L'archive ouverte pluridisciplinaire **HAL**, est destinée au dépôt et à la diffusion de documents scientifiques de niveau recherche, publiés ou non, émanant des établissements d'enseignement et de recherche français ou étrangers, des laboratoires publics ou privés.

Accepted Manuscript

Title: Temperature-dependent viscoelastic modeling of ground deformation: Application to Etna volcano during the 1993-1997 inflation period

Authors: Ciro Del Negro, Gilda Currenti, Danila Scandura

PII: S0031-9201(08)00308-7
DOI: doi:10.1016/j.pepi.2008.10.019
Reference: PEPI 5088

To appear in: *Physics of the Earth and Planetary Interiors*

Received date: 7-3-2008
Revised date: 1-7-2008
Accepted date: 15-10-2008

Please cite this article as: Del Negro, C., Currenti, G., Scandura, D., Temperature-dependent viscoelastic modeling of ground deformation: Application to Etna volcano during the 1993-1997 inflation period, *Physics of the Earth and Planetary Interiors* (2008), doi:10.1016/j.pepi.2008.10.019

This is a PDF file of an unedited manuscript that has been accepted for publication. As a service to our customers we are providing this early version of the manuscript. The manuscript will undergo copyediting, typesetting, and review of the resulting proof before it is published in its final form. Please note that during the production process errors may be discovered which could affect the content, and all legal disclaimers that apply to the journal pertain.



Temperature-dependent viscoelastic modeling of ground deformation: application to Etna volcano during the 1993-1997 inflation period

Ciro Del Negro¹, Gilda Currenti¹, Danila Scandura^{1,2}

¹ *Istituto Nazionale di Geofisica e Vulcanologia, Sezione di Catania, Italy*

² *Dipartimento di Matematica e Informatica, Università di Catania, Italy*

Abstract

We used the Finite Element Method for modeling time-dependent ground deformation due to volcanic pressure sources embedded in a viscoelastic medium. Especially in volcanic areas, the presence of heterogeneous materials and high temperatures produce a lower effective viscosity of the Earth's crust that calls for considering the thermal regime of crustal volume surrounding the magmatic sources. We propose a thermo-mechanical numerical model for evaluating the temperature dependency of the viscoelastic solution. Both temperature distributions and ground deformation are evaluated by solving an axi-symmetric problem to estimate the effects of thermo-viscoelastic response of the medium. The thermo-mechanical model permits to evidence that viscoelastic relaxation is responsible for significant time-dependent variations in long-term deformation. These effects may be relevant for the interpretation and quantitative assessments of the pressure changes within magmatic sources. With this in mind, we reviewed the ground deformation observed on Etna volcano during the 1993-1997 inflation period by setting up a fully 3D temperature-dependent viscoelastic model. Since 1993 different geodetic measurements (EDM, GPS, SAR and leveling data) identified an inflationary phase characterized by a uniform and continuous expansion of the overall volcano edifice that was not perturbed by eruptive activity. The numerical model, including significant viscoelastic material and reduced crustal rigidity around the magmatic source, enables to produce deformation comparable with those obtained from elastic model, requiring a significantly lower pressure. For a purely elastic model with the same geometry and rigidity the pressure change necessary to describe the 1993 through 1997 inflation is around 320 MPa, whereas for the viscoelastic model a pressure increase of about 200 MPa is required.

Keywords: Etna volcano; ground deformation; Finite Element Method; 3D thermo-viscoelastic model.

Introduction

Measuring and interpreting the deformation of volcanoes improve our understanding of how volcanoes work. A variety of processes can cause ground deformation, and being able to recognize and distinguish between them not only broadens our knowledge but is also crucial for

predicting eruptions. Notwithstanding, most volcano deformation models developed to date assume that the Earth's crust behaves as a perfectly elastic solid and allow us to obtain only a simple image of volcanic deformation sources. Over the last decades, elastic numerical models have contributed to assess how medium heterogeneity and topography can influence ground deformation especially near the volcano summit (Cayol & Cornet 1998; Williams & Wadge 2000; Currenti et al., 2008a). All these mechanical deformation models based on an elastic rheology assumption have been successfully and widely applied to interpret geodetic data acquired on several volcanoes (e.g. Walsh & Decker, 1971; Yang et al., 1992; Okada and Yamamoto, 1991; Bonaccorso & Davis, 1999; Currenti et al., 2008b). However, in many cases elastic models seem to be unable to reproduce the observed uplifts unless unrealistic overpressures are considered (e.g. Berrino et al. 1984). In volcanic regions, elastic rheology assumption is oftentimes an overly simplification. The elastic approximation is generally appropriate for small deformations of crustal materials with temperatures cooler than the brittle-ductile transition, between 300 and 500°C depending mainly on composition and strain rate. Although elastic behavior well describes the upper 10-15 km of the Earth's crust, in active volcanic zones viscoelastic behavior is more appropriate to characterize the medium around the magmatic sources, which at relatively shallow crustal levels can extensively perturb the geothermal gradient. Materials surrounding a long-lived magmatic source are heated significantly above the brittle-ductile transition and rocks no longer behave in a purely elastic manner, but permanently deform because of the lower effective viscosity (Newman et al., 2001). Therefore, the thermal state of the volcanoes can greatly influence the surface deformation field, making the elastic approximation inappropriate to model the observed ground deformation.

Some studies on the deformation of a viscoelastic Earth were developed since 1970's, and very slow crustal deformations with the duration time of several days to a few years were investigated (Peltier, 1974). The multi-layer Earth model was rather difficult to deal with analytically, however a simpler case study was anticipated in order to describe the behavior of a viscoelastic half-space. Bonafede et al. (1986) presented the crustal deformation due to the Mogi model in a viscoelastic half-space and worked out analytical solutions for the displacements and associated stress fields induced by a pressure point source. Dragoni and Magnanensi (1989) computed an analytical model considering a spherical magma chamber in an infinite space and surrounded by a homogeneous shell of thermal metamorphic rocks, which is elastic dilatational and Maxwell deviatoric. Recently, Piombo et al. (2007) computed the viscoelastic effect on displacement, displacement gradient and stress fields due to shear and tensile dislocations. Investigations were also conducted using numerical methods, highlighting that rheological heterogeneities may be much more important than elastic heterogeneities in the interpretation of long-term deformation (Folch et al. 2000; Trasatti et al. 2003; Fernandez et al., 2001).

In the present study, we investigated the temporal evolution of the ground deformation caused by a

heating pressurized magma chamber embedded in a viscoelastic heterogeneous medium using Finite Element Method (FEM). We developed a thermo-mechanical model, in which the viscoelastic properties of the medium are derived from the computed temperature distribution. Initially, we carried out several axi-symmetric models to appraise the influence of temperature field on ground deformation. Next, we developed a 3D finite element model to analyze the ground deformation accompanying the 1993-1997 inflation period on Mt Etna. The real topography of volcanic edifice and the crustal heterogeneities inferred from the seismic tomography data were included in the 3D model. We evaluated the effects of conductive thermal propagation on long-term deformation in terms of viscoelastic response of the medium.

Linear Viscoelastic model

The phenomenological behavior of large classes of materials, including elasticity, linear viscosity, and some time-effects, can be studied using analogue models. Simple viscoelastic rheologies can be derived from extrapolations of 1D mechanical models composed of linear combinations of linear springs with spring constant of shear modulus μ and dashpots with coefficient of viscosity η (Currenti et al, 2008c). In such a case analytical solutions can be derived for a homogeneous half-space model using the Correspondence Principle. The computation of the analytical solution is useful to properly set up the numerical model and test the accuracy of the numerical solutions.

Viscoelastic material

We considered linear viscoelastic material in which the stress linearly depends on the strain and its time derivatives. It is usually assumed that the viscous part of the deformation is incompressible, so that the volumetric strain is completely elastic and the viscoelastic deformation may be expressed purely in terms of deviatoric components. Therefore, the bulk modulus $K=E/3(1-2\nu)$ behaves elastically and is simply defined in terms of Young's modulus E and Poisson's ratio ν . In such a case, the rheological constitutive equation can be written as:

$$P(\mathbf{s}) = Q(\mathbf{e}) \quad (1)$$

where \mathbf{s} and \mathbf{e} are the stress and strain deviators respectively (Ivins and Sammis, 1996). P and Q are differential operators expressed as:

$$P = a_m \frac{\partial^m}{\partial t^m} + a_{m-1} \frac{\partial^{m-1}}{\partial t^{m-1}} + \dots + a_0 \quad (2)$$

$$Q = b_m \frac{\partial^m}{\partial t^m} + b_{m-1} \frac{\partial^{m-1}}{\partial t^{m-1}} + \dots + b_0 \quad (3)$$

where a_i and b_i come from the assumed material constants for $i=0, \dots, m$. The differential operators are defined depending on the type of viscoelastic model. Commonly the generalized Maxwell model is represented by a set of M Maxwell models in parallel (Fig. 1). In this case, the operator

may be written as:

$$s = 2G \left(\mu_0 e + \sum_{i=1}^M \mu_i q_i \right), \quad \sum_{i=0}^M \mu_i = 1 \quad (4)$$

where the variable q_i is the solution of differential equation:

$$\dot{q}_i + \frac{1}{\tau_i} q_i = \dot{e} \quad (5)$$

The material is completely defined by assigning the total shear modulus $G=E/2(1+\nu)$ (which is identical to the elastic shear modulus), the fractional shear moduli μ_i and the viscosity η_i for each spring element, leading to the relaxation times $\tau_i=\eta_i/(G\mu_i)$. It is not necessary to specify the fractional modulus μ_0 , since it is obtained by subtracting the sum of the other ratios from one. A number of common material models may be obtained from the generalized Maxwell model by setting the shear moduli of various springs to zero, such as the Maxwell model.

Viscoelastic analytical solution

For a linear viscoelastic material, the solution of the governing equations can be obtained employing the Correspondence Principle (Fung 1965; Christensen 1971), which allows to solve a linear viscoelastic problem using the associated elastic solutions, in which the elastic moduli are replaced by the Laplace transform complex moduli. The Correspondence Principle cannot be applied to a general thermo-viscoelastic problem, but it can be applied to thermo-rheologically simple materials, i.e. when the temperature dependence of mechanical properties is amenable to analytical description, and one of following conditions is satisfied: (i) the temperature field is spatially uniform but time dependent; (ii) the temperature field has a spatial dependence but is independent of time (Christensen, 1982). If the analytic solution for the deformation field of any linear elastic model is given, we can apply the Correspondence Principle to the elastic solution to obtain the viscoelastic behavior of deformation field. The Laplace transform of the viscoelastic solution $\tilde{w}_i(s)$ is given by:

$$\tilde{w}_i(s) = \tilde{g}(s) \tilde{U}_i(s) \quad (6)$$

where $\tilde{g}(s)$ is the Laplace transform of the source time function $g(s)$ giving the temporal evolution of the pressure amplitude, and $\tilde{U}_i(s)$ indicates the displacement function U_i in which the constant moduli are replaced with their Laplace transform moduli. The Laplace transform of the shear modulus, which depends on the particular rheology considered, can be easily obtained using Eq. (1) as:

$$\tilde{\mu}(s) = \frac{G\tilde{Q}(s)}{2\tilde{P}(s)} \quad (7)$$

where $\tilde{Q}_i(s)$ and $\tilde{P}_i(s)$ are the Laplace transforms of Eqs. (2) and (3). For a generalized Maxwell model with M Maxwell linear viscoelastic models in parallel (Fig. 1), the Laplace transform of the

shear modulus is:

$$\tilde{\mu}(s) = G\mu_0 + \sum_{i=1}^M \frac{s}{\frac{s}{G\mu_i} + \frac{1}{\eta_i}} \quad (8)$$

When the shear modulus has been defined and the elastic analytical solution is available, the resulting expression in Eq. (8) must be inverted in order to obtain the viscoelastic solution for the displacement field in the time domain.

Spherical pressure source in a viscoelastic half-space

The elastic analytical solution of a point dilatation source embedded in an elastic and homogeneous half-space was proposed by Mogi (1958). The model well reproduces a finite spherical source if the source depth d is twice compared to the radius a (McTigue, 1987). The elastic displacements are described by the spherical source position, its radius a , and the pressure change ΔP :

$$U_i = \frac{3K + 4\mu}{2\mu(3K + \mu)} \frac{\Delta P a^3 x_i}{R^3} \text{ with } i = 1, 2 \quad U_z = \frac{3K + 4\mu}{2\mu(3K + \mu)} \frac{\Delta P a^3 d}{R^3} \quad (9)$$

where R is the radial distance from the source center to the observation point. We derive the viscoelastic solution applying the Correspondence Principle to Eq. (9). Only the first term in Eq. (9) $(3K+4\mu)/2\mu(3K+\mu)$ depends on the rheology assumption. Adopting a generalized Maxwell rheology with one Maxwell model in parallel and using Eq. (8), the Laplace transform of the shear modulus is given by:

$$\tilde{\mu}(s) = \frac{s(\mu_0 + \mu_1)G + \mu_0\mu_1G^2 / \eta}{s + \mu_1G / \eta} \quad (10)$$

Since we assume that the viscous part of the deformation is incompressible, the bulk modulus $K=E/3(1-2\nu)$ is constant. As source time history, we consider a step-like increase in pressure amplitude at $t=0$ on the source wall:

$$g(t) = \Delta P H(t) = \begin{cases} 0 & t < 0 \\ \Delta P & t \geq 0 \end{cases} \quad (11)$$

where $H(t)$ is the Heaviside function whose Laplace transform is $\Delta P/s$.

To derive the analytical viscoelastic solution we have to multiply the second term of Eqs. (9) with the inverse Laplace transform of the following equation:

$$\tilde{A}(s) = \frac{3K + 4\tilde{\mu}(s)}{2s\tilde{\mu}(s)(3K + 4\tilde{\mu}(s))} \quad (12)$$

which is given by:

$$A(t) = \frac{I}{2G_0} \left[\frac{3K + 4G_0\mu_0}{3K + G_0\mu_0} - 3 \frac{\eta G_0^2 e^{-\frac{G_0\mu_1(3K+G_0\mu_0)t}{\eta(3K+G_0)}}}{\eta(3K + G_0\mu_0)(3K + G_0)} (1 - \mu_0) - \left(\frac{I}{\mu_0} - I \right) e^{-\frac{G_0\mu_0\mu_1 t}{\eta}} \right] \quad (13)$$

For the generalized Maxwell rheology, the viscoelastic response depends on time through two characteristic times:

$$\tau_1 = \frac{3K + G_0}{3K + G_0\mu_0} \tau_0 \quad (14)$$

$$\tau_2 = \frac{\tau_0}{\mu_0} \quad (15)$$

with $\tau_0 = \frac{\eta}{G_0\mu_1}$ the Maxwell time.

Numerical model

The analytical solutions of displacement field in a viscoelastic half-space were used to assess the accuracy of the numerical solutions obtained by Finite Element Method (FEM). We assumed a pressurized spherical source located at 4 km depth with a radius a of 0.7 km and a step-like temporal increase in pressure of $\Delta P = 100$ MPa at $t = 0$. The source is embedded in a homogeneous half-space having Poisson ratio $\nu = 0.25$, total shear modulus $G = 30$ GPa, fractional shear moduli $\mu_0 = \mu_1 = 0.5$, viscosity $\eta = 2 \cdot 10^{16}$ Pa*s giving characteristic times $\tau_0 = 1.33 \cdot 10^6$ s, $\tau_1 = 1.45 \cdot 10^6$ s and $\tau_2 = 2.66 \cdot 10^6$ s.

The numerical analysis needs to set some parameters that could affect the accuracy of the solution. In particular, the size of the computational domain and the size of the finite elements are to be accurately chosen. The domain size is important because of the assignment of finite boundary conditions. We assumed free displacement values at the upper surface and zero displacement values at bottom and lateral boundaries. Since in numerical methods the size domain is finite, these boundary conditions are implemented by considering a domain big enough that the assumption of zero potential at the boundary does not affect the solution in the interested area.

Preliminarily, we considered a 3D axi-symmetric model. In such a case a simpler two dimensional domain can be considered by exploiting the symmetries. Hence, the number of nodes, in which the solution is computed, decreases significantly. This model was chosen to perform a coarser analysis and carry out several tests to assess the goodness of numerical solutions. The FEM model is made up of ~ 16000 triangular elements of variable size, in axi-symmetric configuration. The domain extends 25 km horizontally from the source centre and 35 km below the surface, and well reproduces the conditions generally imposed to half-space models (vanishing stresses at infinity). Computations are carried out by using the commercial software COMSOL Multiphysics,

version 3.3 (Comsol, 2006). Benchmark tests were carried out on the axi-symmetric models in order to verify the accuracy of the numerical solution. For the sake of simplicity, we report only the vertical displacements but similar results are achieved for horizontal displacements. The viscoelastic solution at $t=0$ coincides with the elastic solution. Subsequently, the deformation grows exponentially approaching a finite value. The numerical deformation solution practically coincides with the analytical ones (Fig. 2). This result allowed to validate the numerical technique used in these computations. The ground deformation of the viscoelastic model is enhanced with respect to the elastic solution. Particularly, the ratio between the steady-state viscoelastic solution and the elastic one is about 1.7. Therefore, the inclusion of a viscoelastic rheology significantly lowers the pressures changes, necessary to obtain the same amount of ground deformation, from 100 MPa to 58.9 MPa. To estimate the increase in ground deformation with respect to the elastic solution, we computed the relative misfit for the vertical displacement as:

$$E_{\%} = \frac{\sum |U_{\text{viscoelastic}} - U_{\text{elastic}}|}{\sum |U_{\text{elastic}}|} 100\% \quad (16)$$

The steady-state viscoelastic solution yields a misfit $E_{\%}$ of 71%. In order to get a more realistic result, we used a pressure source that evolves following a trapezoidal source history instead of a step-like source function. Trapezoidal shape function describes the pressurization followed by depressurization of the magmatic source, usually observed in volcanic areas. The source history increases linearly in time from 0 to ΔP for t ranging between 0 and t_1 , remains constant to ΔP for $t_1 \leq t \leq t_2$, and finally decreases from ΔP to 0 for $t_2 \leq t \leq t_3$:

$$g(t) = \Delta P \left\{ \frac{t}{t_1} [1 - H(t - t_1)] + H(t - t_1) - H(t - t_2) + \frac{t_3 - t}{t_3 - t_2} [H(t - t_2) - H(t - t_3)] \right\} \quad (17)$$

whose Laplace transform is:

$$\tilde{g}(s) = \frac{\Delta P}{s^2} \left(\frac{1 - e^{-st_1}}{t_1} + \frac{e^{-st_3} - e^{-st_2}}{t_3 - t_2} \right) \quad (18)$$

Following the procedure described above, we firstly derived the analytical solution and secondly compared it with the numerical one. As shown in Fig. 3, the numerical solution is nearly identical to the analytical one.

The assumption of a homogeneous viscoelastic half-space is too restrictive and limits the application of the model to more realistic case study. In fact, the upper lithosphere does not participate in viscoelastic flow due to its lower temperature. To overcome this limitation, we explore a viscoelastic shell model in which the spherical source is embedded in an elastic half-space and surrounded by a concentric shell of viscoelastic material. It is reasonable to assume that rocks near the inflation source are considerably heated and weakened beyond the brittle-ductile transition temperature, where viscoelastic rheology is more appropriate to describe the mechanical behavior of the surrounding rocks. We supposed a viscoelastic behaviour inside the shell, while an

elastic behaviour outside it. We firstly choose a homogeneous viscoelastic shell with radius 1.7 km. The viscoelastic medium parameters within the shell are the same as in the homogeneous half-space model. As we can notice from Fig. 4, after the introduction of the viscoelastic shell the surface uplift is less enhanced with respect to the previous model when the entire half-space medium is assumed viscoelastic. The relative misfit $E_{\%}$ is decreased to 54%. The amplitude of the viscoelastic response is dependent on the size of the shell (Dragoni and Magnanensi, 1989): wider the shell, higher the deformation observed at the ground surface. Both the thickness and the viscosity of the shell are strongly influenced by the temperature state of the volcanic source.

Temperature-dependent viscoelastic solution

The spatial dependence of viscosity on temperature can be included in the model solving a thermal model to compute the temperature field distribution. Therefore, we conducted a thermo-mechanical model in which the viscoelastic properties of the medium are derived from the computed temperature distribution. We simulated the model in two steps solving separately: (i) the heat conduction equation to compute the temperature profile, and (ii) the viscoelastic problem to obtain the numerical solution of the deformation field.

To derive the temperature profile, we numerically solved the heat conduction equations in an axial symmetric formulation, given by:

$$\nabla \cdot (k \nabla T) = -A \quad (19)$$

where $T=T(r,z)$ is the temperature field, r is the radial coordinate, z is the vertical coordinate, k is thermal conductivity, and $A(z)=A_s \exp(-z/b)$ is the crustal volumetric heat production, where A_s is the volumetric rate of heat production, and b is a characteristic depth of the order of 10 ± 5 km. Since the deformation timescales are much shorter than those over which the magma chamber evolution takes place, the temperature distribution, and therefore the viscosity profile inside the shell, can be considered as steady. As boundary condition at the ground surface, we assumed that the surface is kept constant at atmospheric temperature, since the thermal conductivity of the air is much smaller than that of the ground. At bottom and lateral boundaries we assigned the geothermal temperature values, because they are far enough to not be affected by the magmatic source. We used the steady-state geothermal profile given by (Ranalli, 1995; Turcotte and Schubert, 1982):

$$T(z) = T_s + \left(\frac{q_m z}{k} \right) + \left(\frac{A_s b^2}{k} \right) (1 - e^{-z/b}) \quad (20)$$

where T_s is the surface temperature, q_m is the heat flow coming from the mantle. The temperature on the magma wall was set to $T_0=1000$ K. Physically, this boundary condition is equivalent to stating that the magma walls act as heat sources, simulating a continuous refilling of the magma chamber (Dragoni et al., 1997; Civetta et al., 2004).

Starting from the temperature distribution, a variety of empirical relationships can be used to infer the temperature-viscosity dependence. We estimated the medium viscosity surrounding the source region using the Arrhenius formula:

$$\eta = A_D \exp\left(\frac{E}{RT}\right) \quad (21)$$

where A_D is the Dorn parameter, E is the activation energy, R is the Boltzmann constant, and T the absolute temperature. Additional work is needed to define plausible values for the rheological parameters, and determine the extent to which these parameters vary in the region of high thermal gradients near the magma chamber. The values of the parameters used in the computations are summarized in Table I. The viscosity inside the shell depends on the temperature distribution. However, the thickness of the shell was kept constant at 1.7 km.

Several simulations were also conducted to investigate how the temperature of the magmatic source affects the ground uplift. Different values of temperature in the range 1000-1500 K were used. The steady-state temperature profiles using $T=1000$ K and $T=1500$ K at the source wall are shown in Fig. 5 together with the estimated medium viscosity from Eq. (21). The viscosity within the viscoelastic shell is ranging from 10^{15} Pas to 10^{20} Pas for $T=1000$ K, and from 10^{13} Pas to 10^{17} Pas for $T=1500$ K (Fig. 5). The amplitude of the deformation after 120 days is dependent on the temperature profile (Fig. 6). The vertical uplift at the ground surface above the source center varies from 6.9 cm at 1000 K to 7.9 cm at 1500 K with a relative misfit $E_{\%}$ of 29% and 47%, respectively (Fig. 7). However, the increase is not linearly proportional, but a saturation effect is observed for higher temperatures. This could be ascribed to the fixed dimension of the shell and to the exponential dependency of the viscosity on the temperature. It is reasonable to assume that the thickness of the viscoelastic shell increases with the temperature.

The viscoelastic behaviour is appropriate around the magmatic source where the temperature is higher. Instead of using a constant thickness for the viscoelastic spherical shell, we modified the properties of the medium through the constitutive equations, allowing the element of the domain to behave elastically or viscoelastically in function of the temperature distribution. We associated to the medium elastic properties where the temperature values are below a fixed threshold and viscoelastic properties above this threshold. The solutions vary as a function of the threshold. We made a comparison between this model in which the thickness of the shell is temperature dependent and the model in which all the medium is fully viscoelastic. We observed that these results does not differ too much using temperature threshold lower than 700 K (Fig. 8). Far away from the source, the temperature decays, yielding a higher value of viscosity which makes the medium to behave as elastically (Williams and Richardson, 1991). As before, the deformation raises with temperature (Fig. 9), but no saturation phenomena are observed (Fig. 10). The vertical uplift at the ground surface above the source center reaches, after 120 days, a deformation of 7.4 cm at 1000 K ($E_{\%} = 38\%$) and 8.8 cm at 1500 K ($E_{\%} = 59\%$). It is worth to note that in this case the

deformation is enhanced with respect to the case in which the viscoelastic behavior is restricted to a fixed shell around the source. The temporal evolutions of the vertical uplift with source wall temperature at $T=1000$ K and $T=1500$ K are shown in Fig. 11. As the temperature increases, the viscoelasticity decreases yielding lower relaxation times (Fig. 11) and the ground deformation raises faster. Even when the viscoelastic shell thickness is fixed (Fig. 11a), the temperature profile affects the amount of deformation reached after the exponential increase. When the rheological behavior of the whole surrounding medium is temperature-dependent (Fig. 11b), the region, which behaves viscoelastically, becomes wider as the temperature increases and gives more contribution to the viscoelastic part of the deformation field.

An application to Etna volcano

We extended the finite element method, used for the axi-symmetric model, to a fully 3D formulation to study the long-term deformation observed at Mt Etna in 1993-1997 period. Etna is one of the better monitored and successfully studied volcanoes in the world, where continuously running geodetic networks are operating (Bonaccorso et al. 2004). Since 1993, different geodetic techniques (EDM, GPS, SAR and leveling data) identified an inflation phase characterized by a uniform expansion of the overall volcano edifice. The beginning of the inflation phase was detected from the comparison of SAR images covering the 1993-1995 time interval. The inversion of interferograms required the inflation from a spheroidal magmatic source located at about 5 km bsl (Lundgren et al., 2003). Also levelling data supported the presence of a pressurized spherical source beneath the summit craters at 4.5 km bsl (Obrizzo et al., 2004). Recently, Bonaccorso et al. (2005) interpreted the 1993-1997 GPS and EDM data by a pressurized ellipsoidal source using a numerical elastic model. In order to reproduce the observed displacements, an effective overpressure of about 320 MPa was needed, which is exceedingly high. The inclusion of a realistic viscoelastic component could significantly lower the inferred pressure necessary to explain the observed surface deformation (Newman et al., 2006). With this in mind, we reviewed the 1993-1997 inflation phase on Mt Etna using a 3D thermo-viscoelastic numerical model. We adopt the same ellipsoidal source determined by Bonaccorso et al. (2005), which is located 4.2 km bsl beneath the central craters (latitude 4177.9 UTM km and longitude 500.7 UTM km). The ellipsoid has a semi-major axis of 1854 m and the other two semi-axes of 725 m and 544 m, respectively with an orientation angle of 124° and a dip angle of 77° . In the numerical model we also included the rheological heterogeneities of the medium. Instead of using a simple multi-layered crustal rigidity model, a complex distribution of rheological medium properties was considered (Currenti et al., 2007). We used P-wave and S-wave seismic velocities, inferred from recent seismic tomography studies (Chiarabba et al., 2000; Patanè et al., 2006), to derive the elastic medium parameters. Particularly, the Young modulus was estimated by using the following equation

(Kearey and Brooks, 1991):

$$E = 2V_s^2 \rho(1 + \nu) \quad (22)$$

where V_s is the seismic S-wave propagation velocity, and ρ is the density of the medium which was fixed to 2500 kg/m^3 . Instead, the values of Poisson ratio were obtained using the equation (Kearey and Brooks, 1991)

$$\nu = [(V_p / V_s)^2 - 2] / [2(V_p / V_s)^2 - 2] \quad (23)$$

where V_p is the seismic P-wave propagation velocity. On the basis of Eqs. (22) and (23), the Young modulus varies from 11.5 GPa to 133 GPa, while the Poisson ratio is in the range 0.12-0.32.

The 3D model drastically increases the computational load. In this case, no symmetries can be exploited and the number of elements and nodes hugely increases. The procedure for computing the viscoelastic deformation field is the same as for the previous axi-symmetric model. The computational domain was set up to a large volume extending $100 \times 100 \times 100 \text{ km}^3$ in order to avoid artifacts in the numerical solution because of the proximity of the boundary. The mesh of the ground surface was generated using a digital elevation model of Etna volcano from the 90 m Shuttle Radar Topography Mission (SRTM) data. The computational domain was represented by number of 20000 arbitrarily distorted tetrahedral elements connected by 4000 nodes. The mesh resolution is about 100 m around the ellipsoidal source, about 300 m in the area surrounding the volcano edifice, and decreases to 2 km in the far field. Firstly, we solved the conductive heat transfer equation. As thermal boundary condition, a steady-state geothermal profile was set up along the bottom and lateral boundaries. A vertical geothermal gradient of $22 \text{ }^\circ\text{C/km}$ was assumed for the areas surrounding the volcano edifice in agreement with the temperature measurements carried out in deep boreholes (AGIP, 1977). A continuous refilling of the magma chamber was simulated by setting the temperature on the ellipsoidal source wall. We performed two simulations using $T=1000 \text{ K}$ and $T=1500 \text{ K}$ to understand the role played by the temperature values on the source wall. The temperature profile was used to compute the viscoelasticity of the overall domain. Then, we solved the mechanical viscoelastic model using the computational scheme described in the axi-symmetric model. The comparison between the elastic solutions and the viscoelastic response after about 3 years and half are shown in Fig. 12.

Two other simulations were carried out. In the first one we assumed a step-like pressure change, in the second one we assumed a linear pressure increase in order to simulate the continuous inflation phase of the pressurized magmatic source. The pressure source evolves like a ramp function from 0 MPa to 320 MPa during 1993-1997 with a increment of 90 MPa/year. Even if the temporal evolution is very different, the final uplift is quite similar (Fig. 13). Therefore, a comparison with the temporal evolution of real data could allow for distinguishing between them. In Bonaccorso et al. 2005, no temporal evolution of ground deformation data was shown. However, a cumulative

planar areal dilatation was computed for the Etna networks. Since a fairly continuous expansion seems to affect the volcanic edifice starting from 1993 to 1997, we can better consider a continuous linear feeding rate of the pressure source.

The relative misfit with respect to the elastic solution at the ground surface is 55% for a wall temperature of $T=1000$ K and 66% for $T=1500$ K. Both the horizontal and vertical deformation in the viscoelastic solution are enhanced of about 1.6 in comparison with the elastic solution. Therefore, the temperature-dependent viscoelastic model requires a lower pressure changes (~ 200 MPa) that is nearer to the lithostatic load (~ 170 MPa), but still higher than the crustal strength (~ 45 MPa).

Discussion and Conclusions

Numerical models have been carried out to investigate the temporal evolution of viscoelastic deformation caused by pressure changes within a magmatic source. The presence of viscoelastic material, which likely characterizes the crust around magmatic sources, greatly alters the deformation field. We found out that the ground uplift grows in time and its temporal evolution is mainly dependent on the average rigidity and viscosity of the medium surrounding the source.

Initially, we assumed a spherical source embedded in a homogeneous viscoelastic half-space model with a generalized Maxwell rheology. In this simple case, we derived the analytical viscoelastic solution applying the Correspondence Principle. It allowed to compare the numerical solution with the analytical one to verify the accuracy of the numerical method. The homogeneity assumption is an overlay simplification that was overcome with the introduction of a viscoelastic spherical shell around the magmatic source and an elastic medium outside it. However, the thickness and the viscosity of the spherical shell depend on the magma temperature and the thermal state of the surrounding rocks. The definition of elastic\anelastic rock properties cannot disregard the thermal regime of the crust especially in volcanic regions. To this aim, we examined the effect of magma source temperature on viscoelastic deformation implementing a thermo-mechanical model. The simulations evidenced that the thermal state of the crust influences both the temporal evolution of deformation field, in terms of relaxation time, and the amplitudes of the steady-state ground deformation.

Successively, we extended the procedure to a fully 3D model to investigate the effects of viscoelastic rheologies surrounding a pressurized prolate spheroid source during the inflation period of time-dependent deformation occurred at Mt Etna between 1993 and 1997. This period of increasing pressurization of the plumbing system was not perturbed by eruptive activity, which resumed afterward in 1998 from the summit craters (Bonaccorso et al., 2005). The viscoelastic model enables to produce deformation comparable with those obtained from elastic model, requiring a significantly lower pressure. For a purely elastic model with the same geometry and rigidity the pressure change necessary to describe the 1993 through 1997 inflation is around 320

MPa, whereas for the viscoelastic model a pressure increase of about 200 MPa is required. Nevertheless, the pressure change is still high. Since no eruption had occurred, the overall pressure change should remain below the lithostatic load. Assessing source pressure is essential for improving the knowledge of the physics of volcano deformation and eruption hazard. Because of the strict link between crustal rigidity and source pressure, a lack of insight into the rheology can increase the uncertainty on source volumes and associated pressures (Newman et al., 2001). Moreover, Trasatti et al. (2007) showed that the presence of heterogeneities strongly modify the position of the pressure sources inferred by numerical inversion. Therefore, the rheology assumption strongly affects the estimates of both pressure and position.

In order to validate thermal and mechanical numerical models it is necessary to have a more complete overall picture of the thermal state and the elastic/anelastic rock properties in the crust of Mt Etna. The medium heterogeneity, estimated from the 3D velocity model, can be significantly affected by: (i) the low spatial resolution of 3 km in the tomography model by Chiarabba et al. (2000), (ii) the variation of 3D velocity model in the analyzed period, (iii) the difference between the static elastic modulus and the dynamic elastic modulus deduced from the P-wave velocity. Patanè et al. (2006) obtained new 3D velocity models at higher resolution on Mt Etna, detecting significant variations in the elastic parameters during different volcanic cycles. A correction factor of 0.7 can be used to account for the difference between the static and dynamic moduli at confining pressure of about 100 MPa. That would also contribute to a proportional decrease in the source pressure to 140 MPa. Therefore, the inclusion of significant viscoelastic material and lower crustal rigidity near a magmatic source, which is geologically expected, can considerably reduce the pressure necessary to produce the observed surface deformation.

The thermal parameters involved in the thermo-mechanical model can be better constrained using temperature data, when available, and seismic attenuation tomography. The study of attenuation of seismic waves can provide a more realistic image of the thermal regime in the upper crust inside the Mt Etna. Laboratory measurements in the seismic frequency range indicate an exponential Arrhenius-law type increase of intrinsic attenuation with the temperature of the rocks (Kampfmann and Berckemer, 1985). Several recent works (Arevalo et al., 2005; De Gori et al., 2005; Patanè et al., 2006) have shown that the imaging of V_p/V_s and quality factor Q_p could be useful tools to define location and extension of melt or highly fractured materials accompanying the volcanic activity at Mt Etna. On the west of the high rigidity body recognized beneath the South-East flank of Etna volcano, De Gori et al. (2005) hypothesized a shallow broad region of low Q_p hot fluids, which is in agreement with the location of the estimated ellipsoidal source. With the inclusion of temperature distribution coming from local temperature T and Q_p relationship, we will be capable of performing more realistic numerical simulations.

ACKNOWLEDGMENTS

This study was undertaken with financial support from the ETNA project (DPC-INGV 2004–2006 contract) and the VOLUME project (European Commission FP6-2004-Global-3). This work was developed in the frame of the TecnoLab, the Laboratory for the Technological Advance in Volcano Geophysics organized by DIEES-UNICT and INGV-CT. We are grateful to Giuliano Cammarata and Giuseppe Petrone from Catania University for making available the computational resources to perform the computations of the 3D numerical model. We thank the editor Mark Jellinek, Michele Dragoni and an anonymous reviewer for their useful comments on this paper.

References

- AGIP S.p.A., 1977. Temperature sotterranee. Grafiche Fili Brugora, Milano, p. 1390.
- Arevalo, C. M., Patanè, D., Rietbrock, A., Ibanez, J. M., 2005. The intrusive process leading to the Mt. Etna 2001 flank eruption: Constraints from 3-D attenuation tomography. *Geophys. Res. Lett.*, 32, doi:10.1029/2005GL023736.
- Berrino G., Corrado G., Luongo G., Toro B., 1984, Ground Deformation and Gravity Changes Accompanying the 1982 Pozzuoli Uplift. *Bull. Volcanol.* 47-2, 187-200.
- Bonaccorso, A., Davis, P. M., 1999. Models of ground deformation from vertical volcanic conduits with application to eruptions of Mount St. Helens and Mount Etna. *Geophys. Res. Lett.*, 104(B5), 10531–10542.
- Bonaccorso, A., Davis, P. M., 2004. Modeling of ground deformation associated with recent lateral eruptions: Mechanics of magma ascent and intermediate storage at Mt. Etna, in *Mount Etna Volcano Laboratory*. Vol. 143, edited by A. Bonaccorso, S. Calvari, M. Coltelli, C. D. Negro, and S. Falsaperla, p. 384, American Geophysical Union Monography Series.
- Bonaccorso, A., Cianetti, S., Giunchi, C., Trasatti, E., Bonafede, M., Boschi E., 2005. Analytical and 3D numerical modeling of Mt. Etna (Italy) volcano inflation. *Geophys. J. Int.*, 163, 852-862.
- Bonafede, M., Dragoni, M., Quarenì, F., 1986. Displacement and stress fields produced by a centre of dilatation and by a pressure source in a viscoelastic half-space: application to the study of ground deformation and seismic activity at Campi Flegrei, Italy. *Geophys. J. R. astr. Soc.*, 87, 455-485.
- Cayol, V., Cornet, F.H., 1998. Effects of topography on the interpretation of the deformation field of prominent volcanoes, Application to Etna. *Geophys. Res. Lett.*, 25, 1979–1982.
- Chiarabba, C., Amato, A., Boschi, E., Barberi, F., 2000. Recent seismicity and tomographic modeling of the Mount Etna plumbing system. *J. Geophys. Res.*, 105, 10923-10938.
- Christensen, R. M., 1971. *Theory of Viscoelasticity: An Introduction*. Academic Press, New York.
- Christensen, R. M., 1982. *Theory of viscoelasticity: An introduction*. pp. 364 , Academic San Diego Calif.
- Comsol Multiphysics 3.3, 2006. Comsol AB, Stockholm, Sweden.

- Civetta, L., D'Antonio, M., De Lorenzo, S., Di Renzo, V., Gasparini, P., 2004. Thermal and geochemical constraints on the 'deep' magmatic structure of Mt. Vesuvius. *J. Volcanol. Geotherm. Res.*, 133, 1-12.
- Currenti, G., Del Negro, C., Ganci, G., 2007. Modelling of ground deformation and gravity fields using finite element method: an application to Etna volcano. *Geophys. J. Int.*, doi: 10.1111/j.1365-246X.2007.03380.x.
- Currenti, G., Del Negro, C., Ganci, G., Scandura, D., 2008a. 3D numerical deformation model of the intrusive event forerunning the 2001 Etna eruption. *Phys. Earth Planet. Interiors*, doi:10.1016/j.pepi.2008.05.004
- Currenti, G., Del Negro, C., Ganci, G., Williams, C.A., 2008b. Static stress changes induced by the magmatic intrusions during the 2002-2003 Etna eruption, submitted to *J. Geophys. Res.*
- Currenti, G., Del Negro, C., Sasai, Y., 2008c. Time dependent piezomagnetic fields in viscoelastic medium, *Geophys. J. Int.*, 172, 536–548 doi:10.1111/j.1365-246X.2007.03679.x.
- De Gori, P., Chiarabba, D., Patanè, 2005. Qp structure of Mt. Etna: constraints for the physics of the plumbing system. *J. Geophys. Res.*, 110, doi:10.1029/2003JB002875.
- Dragoni, M. and Magnanensi, C., 1989. Displacement and stress produced by a pressurized, spherical magma chamber, surrounded by a viscoelastic shell *Phys. Earth Planet. Interiors*, 56, 316-328.
- Dragoni, M., Harabaglia, P., Mongelli, F., 1997. Stress Field at a Transcurrent Plate Boundary in the Presence of Frictional Heat Production at Depth. *Pure appl. geophys.*, 150, 181-201.
- Fernández, J., Tiampo, K. F., Rundle, J. B., 2001. Viscoelastic displacement and gravity changes due to point magmatic intrusions in a gravitational layered solid earth. *Geophys. J. Int.*, 146, 155-170.
- Folch, A., Fernández, J., Rundle, J. B., Martí, J., 2000. Ground deformation in a viscoelastic medium composed of a layer overlying a half-space: a comparison between point and extended sources. *Geophys. J. Int.*, 140, 37-50.
- Fung, Y.C., 1965. *Foundations of solid Mechanics*, Prentice-Hall, Englewood Cliffs.
- Kampfmann, W., Berckemer, H., 1985. High temperature experiments on the elastic and anelastic behaviour of magmatic rocks. *Phys. Earth Planet. Interiors* 40, 223–247.
- Kearey, P., Brooks, M., 1991. *An introduction to geophysical exploration*. Second edition. Blackwell Scientific Publications, Oxford, pp. 254.
- Ivins, E. R., Sammis, C. G., 1996. Transient creep of a composite lower crust, *J. Geophys. Res.*, 101(B12), 27981-28004.
- Lundgren, P., P. Berardino, M. Coltelli, G. Fornaro, R. Lanari, G. Puglisi, E. Sansosti, M. Tesaro (2003), Coupled magma chamber inflation and sector collapse slip observed with synthetic aperture radar interferometry on Mt. Etna volcano. *J. Geophys. Res.*, 108(B5), 2247, doi:10.1029/2001JB000657.

- McTigue, D.F., 1987. Elastic stress and deformation near a finite spherical magma body: resolution of the point source paradox. *J. Geophys. Res.*, 92, 12 931–12 940.
- Mogi, K., 1958. Relations between the eruptions of various volcanoes and the deformations of the ground surfaces around them. *Bull. Earthq. Res. Inst., Univ. Tokyo*, 36, 99-134.
- Newman, A. V., T. Dixon, G. Ofoegbu, J. Dixon, 2001. Geodetic data constraints on recent activity at Long Valley Caldera, California: evidence for viscoelastic rheology. *J. Volcan. Geoth. Res.*, 105, 183–206.
- Newman, A. V., Dixon, T. H., Gourmelen N., 2006. A four-dimensional viscoelastic deformation model for Long Valley Caldera, California, between 1995 and 2000, *J. Volcanol. Geotherm. Res.*, 150, 244-269.
- Obrizzo, F., Pingue, F., Troise, C., De Natale, G., 2004. Bayesian inversion of 1994-98 vertical displacements at Mt. Etna; evidence for magma intrusion. *Geophys. J. Int.*, 157(2), 935–946, doi:10.1111/j.1365-246X.2004.02160.x.
- Okada, Y., Yamamoto, Y., 1991. Dyke intrusion model for the 1989 seismovolcanic activity of Off Ito, Central Japan. *J. Geophys. Res.* 96, 10361-10376.
- Patanè, D., Barberi, G., Cocina, O., De Gori, P., Chiarabba, C., 2006. Time-Resolved Seismic Tomography Detects Magma Intrusions at Mount Etna. *Science*, 313, 821-823.
- Peltier, W.R., 1974. The impulse response of a Maxwell earth. *Rev. Geophys. Space Phys.*, 12, 649–669.
- Piombo, A., Tallarico, A., Dragoni, M., 2007. Displacement, strain and stress fields due to shear and tensile dislocations in a viscoelastic half-space. *Geophys. J. Int.*, doi: 10.1111/j.1365-246X.2007.03283.x.
- Ranalli, G., 1995. *Rheology of the Earth*, pp. 413, Chapman and Hall, London.
- Trasatti, E., C. Giunchi, M. Bonafede, 2003. Effects of topography and rheological layering on ground deformation in volcanic regions. *J. Volcanol. Geotherm. Res.*, 122, 89–110.
- Trasatti, E., C. Giunchi, N. Piana Agostinetti, 2007. Numerical inversion of deformation caused by pressure sources: application to Mount Etna (Italy). *Geophys. J. Int.*, doi:10.1111/j.1365-246X.2007.03677.x.
- Turcotte, D. L. Schubert, G., 1982. *Geodynamics – Applications of continuum physics to geological problems*, Wiley, New York.
- Walsh, J.B., Decker, R.W., 1971. Surface deformation associated with volcanism. *J. Geophys. Res.* 76, 3291-3302.
- Williams, C. A., Richardson, R. M., 1991. A rheologically layered three-dimensional model of the San Andreas fault in central and southern California. *Geophys. Res. Lett.*, 25, 1549-1552.
- Williams, C. A. Wadge, G., 2000. An accurate and efficient method for including the effects of topography in three-dimensional elastic models of ground deformation with applications to radar interferometry. *J. Geophys. Res.*, 105, 8103-8120.

Yang, X., Davis, P.M., Delaney, P.T., Okamura, A.T., 1992. Geodetic analysis of dike intrusion and motion of the magma reservoir beneath the summit of Kilauea volcano, Hawaii: 1970-1985. *J. Geophys. Res.* 97, 3305-3324.

Table I - Thermal and mechanical parameters.

Thermal parameters		
T_s	Surface temperature	273 K
q_m	Heat flow	0.03 mWm ⁻²
k	Thermal conductivity	4 Wm ⁻¹ K ⁻¹
A_s	Volumetric rate of heat production	2.47 10 ⁻⁶ Wm ⁻³
b	Length scale for crustal radioactive decay	14.170 km
Mechanical parameters		
A_D	Dorn parameter	10 ⁹ Pas
E	Activation energy	120 kJ/(mol)
R	Boltzmann constant	8.314 J/(mol K)

Figure Captions

Figure 1 - Generalized Maxwell model.

Figure 2 - Comparison between analytical solutions (solid line) and numerical results (circles) for the vertical uplift due to a spherical pressure source in a homogenous and viscoelastic half-space.

Figure 3 - Comparison between analytical solution (solid line) and numerical result (circles) for the ground uplift as a function of time. A trapezoidal source history is assumed with $t_1 = \tau_0/2$, $t_2 = 5\tau_0$ and $t_3 = 5.5\tau_0$. The pressure reaches 100 MPa.

Figure 4 – Ground uplift due to a spherical pressure source embedded in a viscoelastic half-space (solid line) and in an elastic half-space and surrounded by a viscoelastic shell (circles).

Figure 5- Temperature (color scale) and viscosity (contour lines in Pas) profiles for source wall temperature at $T=1000$ K (on the left) and $T=1500$ K (on the right).

Figure 6 - Vertical uplift at 120 days after the pressure increase within a magma source embedded in an elastic medium and surrounded by a viscoelastic spherical shell. Different thermal regimes are considered.

Figure 7 – Misfit on the vertical uplift between the elastic solution and the viscoelastic response at 120 days after the pressure step-like increase. The uplift increases with the temperature on the source wall.

Figure 8 - Comparison between the model in which the thickness of the shell is temperature dependent (dashed line) and the model in which all the medium is fully viscoelastic (solid line). **Figure 9** - Vertical uplift at 120 days after the pressure increase within a magma source embedded in a temperature-dependent viscoelastic half-space. The temperature on the source wall is varied from 1000 K to 1500 K.

Figure 10 - Misfit on the vertical uplift between the elastic solution and the viscoelastic solution at 120 days after the pressure increases. The viscoelastic response is strongly dependent on the temperature along the source wall.

Figure 11 – Ground uplift at $r=0$ as function of time. (a) The pressure source is surrounded by a viscoelastic spherical shell and the wall temperature is $T=1000$ K (solid line) and $T=1500$ K (dashed line). (b) The pressure source is embedded in a temperature-dependent viscoelastic half-space and the wall temperature is $T=1000$ K (solid line) and to $T=1500$ K (dashed line).

Figure 12 – Comparison between GPS observed (black) and computed deformation during the 1993-1997 period. The numerical computations are performed assuming a heterogeneous elastic medium (blue, after Bonaccorso et al., 2005) and a temperature-dependent viscoelastic medium with pressure source of 320 MP and source wall temperature at either 1000 K (green) or 1500 K (red).

Figure 13 – Vertical uplift at OBS (circle), ESLN (square) and TDF (diamond) computed for a step-like pressure increase (black lines) and linear pressure change (grey lines).

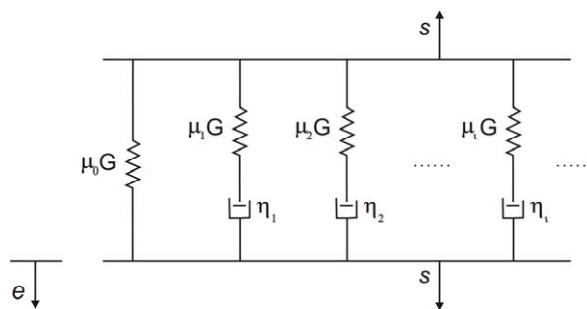


Figure 1 – Generalized Maxwell model.

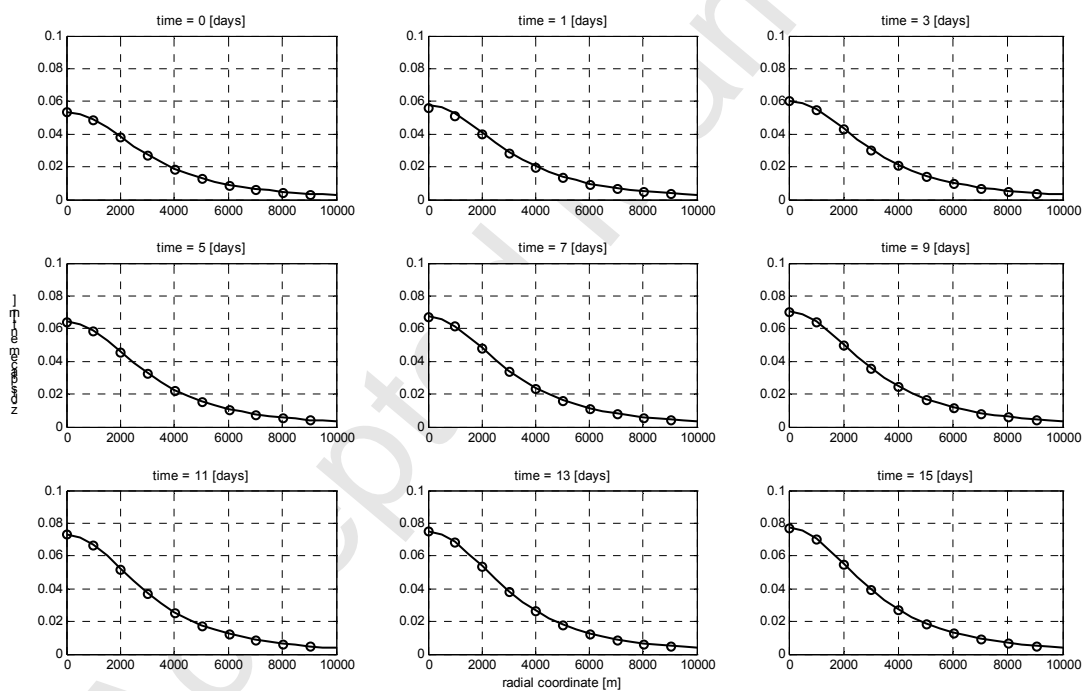


Figure 2 - Comparison between analytical solutions (solid line) and numerical results (circles) for the vertical uplift due to a spherical pressure source in a homogenous and viscoelastic half-space.

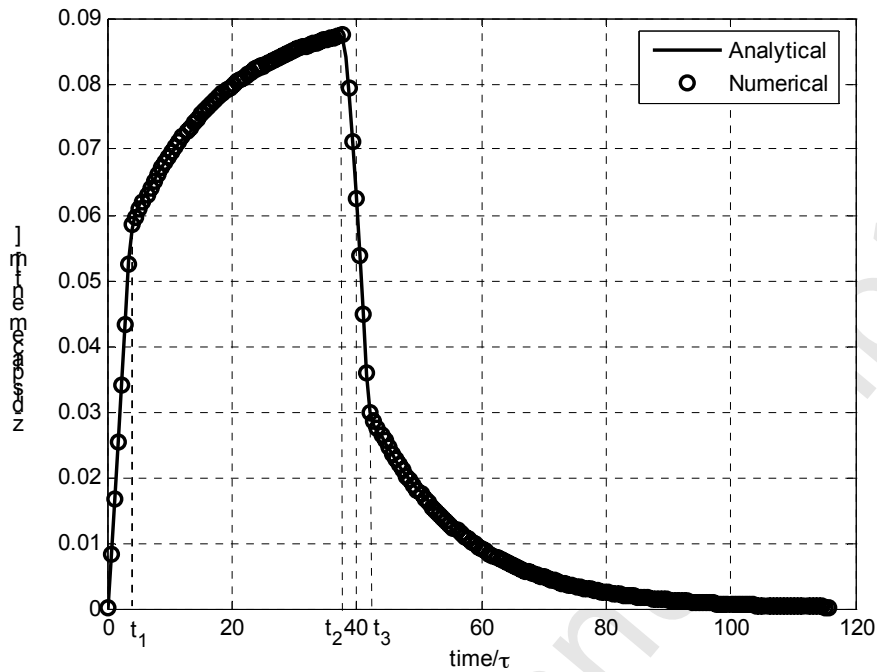


Figure 3 - Comparison between analytical solution (solid line) and numerical result (circles) for the ground uplift as a function of time. A trapezoidal source history is assumed with $t_1 = \tau_0/2$, $t_2 = 5\tau_0$ and $t_3 = 5.5\tau_0$. The pressure reaches 100 MPa.

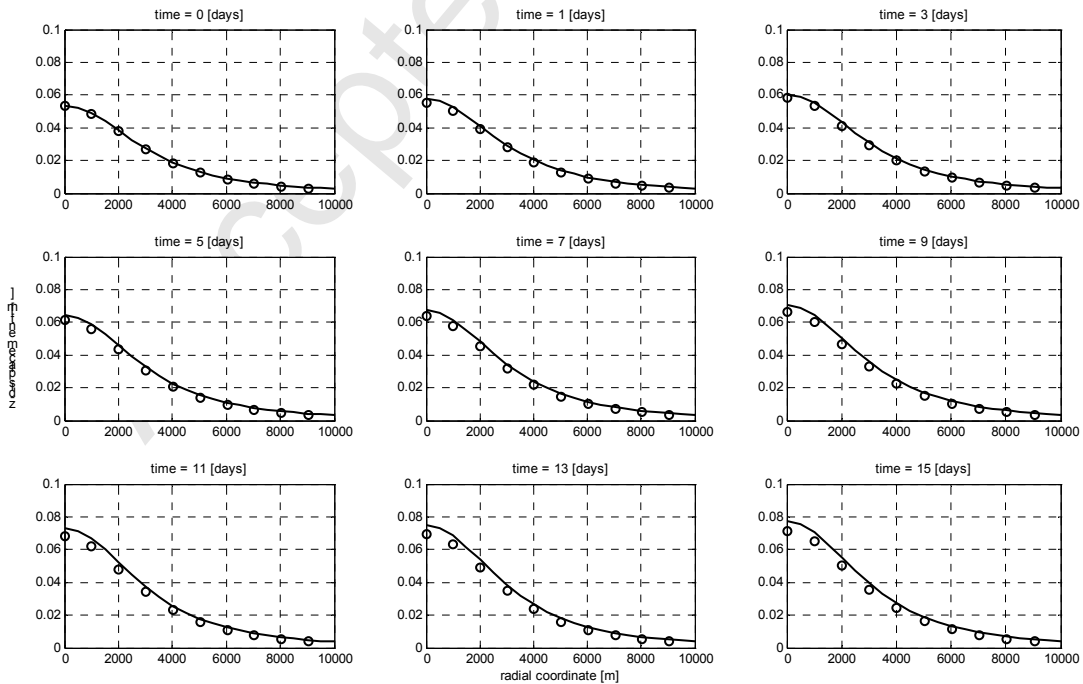


Figure 4 – Ground uplift due to a spherical pressure source embedded in a viscoelastic half-space (solid line) and in an elastic half-space and surrounded by a viscoelastic shell (circles).

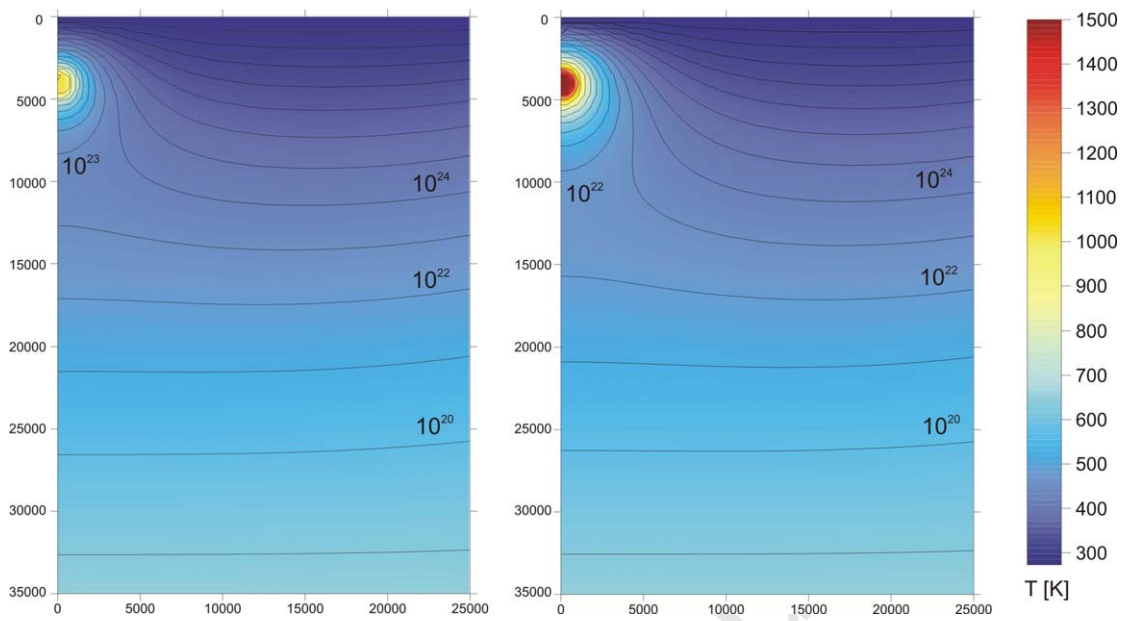


Figure 5- Temperature (color scale) and viscosity (contour lines in Pas) profiles for source wall temperature at $T=1000$ K (on the left) and $T=1500$ K (on the right).

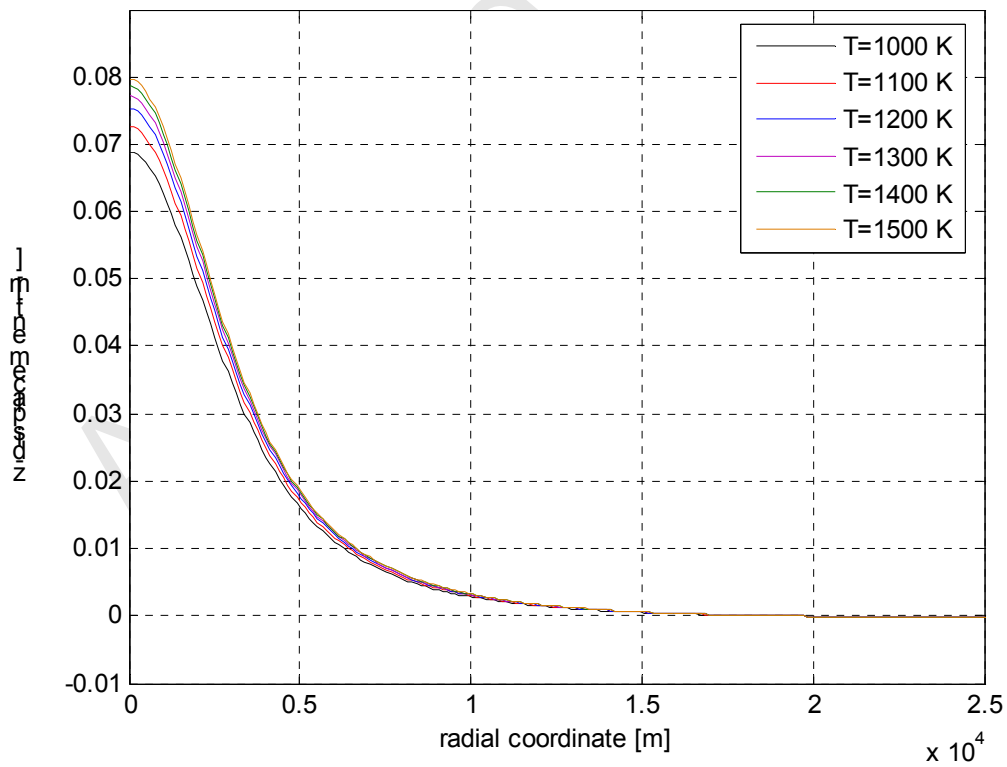


Figure 6 - Vertical uplift at 120 days after the pressure increase within a magma source embedded in an elastic medium and surrounded by a viscoelastic spherical shell. Different thermal regimes are considered.

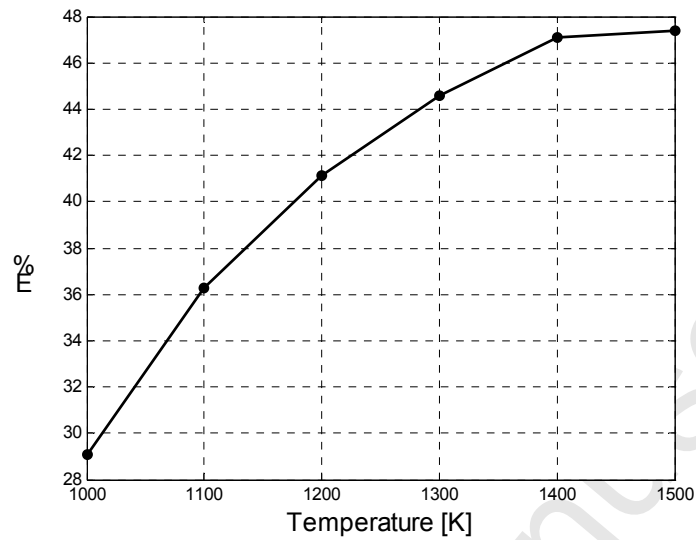


Figure 7 – Misfit on the vertical uplift between the elastic solution and the viscoelastic response at 120 days after the pressure step-like increase. The uplift increases with the temperature on the source wall.

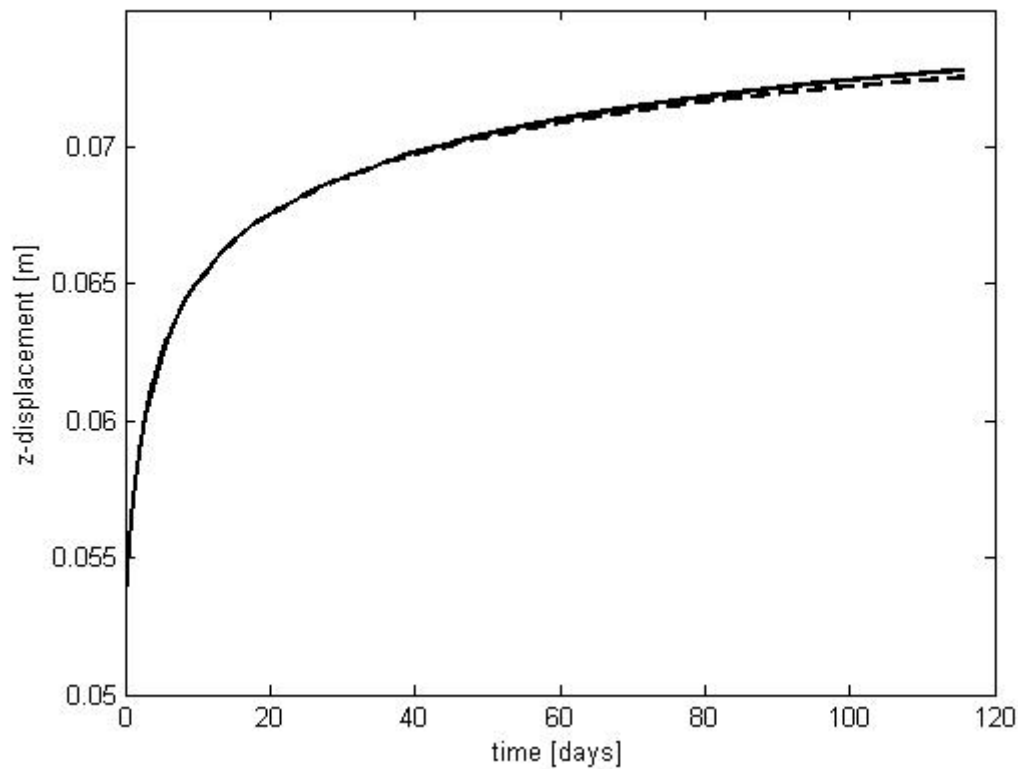


Figure 8 - Comparison between the model in which the thickness of the shell is temperature dependent (dashed line) and the model in which all the medium is fully viscoelastic (solid line).

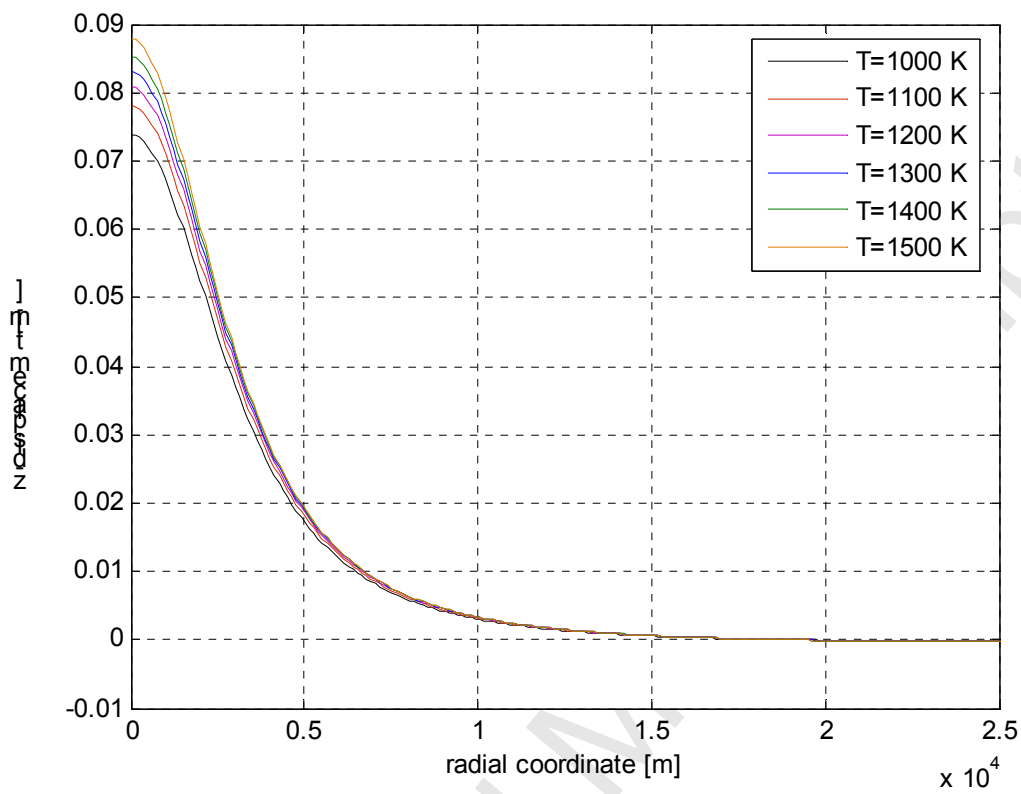


Figure 9 - Vertical uplift at 120 days after the pressure increase within a magma source embedded in a temperature-dependent viscoelastic half-space. The temperature on the source wall is varied from 1000 K to 1500 K.

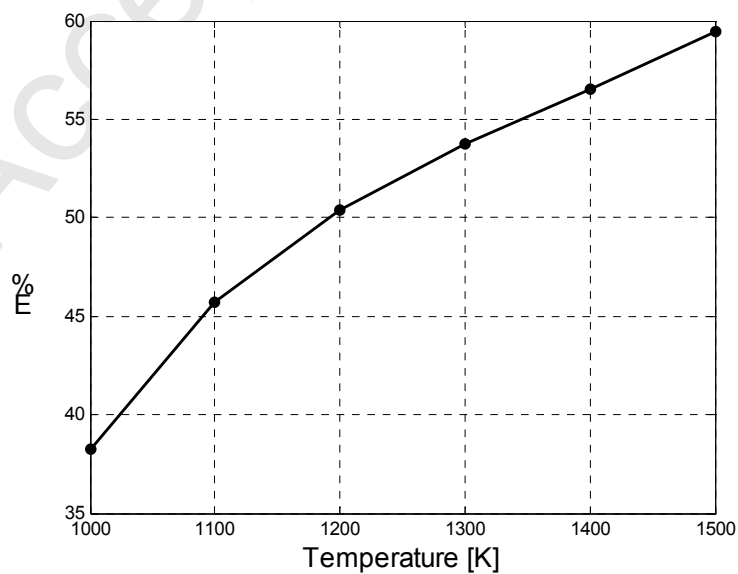


Figure 10 - Misfit on the vertical uplift between the elastic solution and the viscoelastic solution at 120 days after the pressure increases. The viscoelastic response is strongly dependent on the temperature along the source wall.

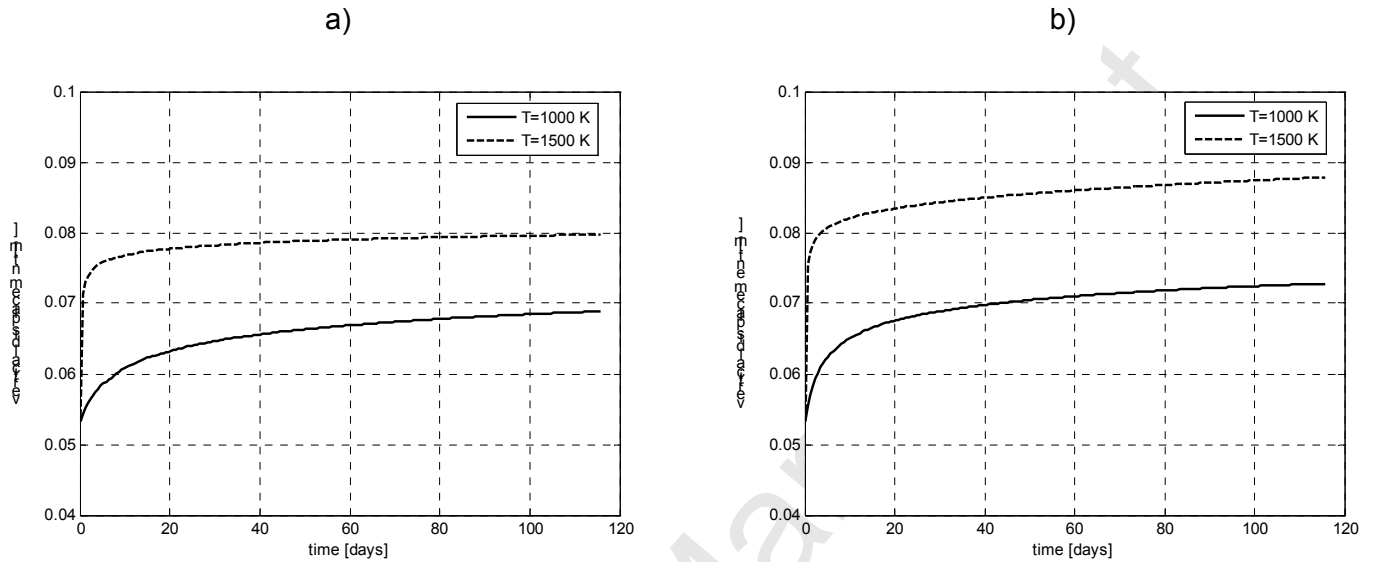


Figure 11 – Ground uplift at $r=0$ as function of time. (a) The pressure source is surrounded by a viscoelastic spherical shell and the wall temperature is $T=1000$ K (solid line) and $T=1500$ K (dashed line). (b) The pressure source is embedded in a temperature-dependent viscoelastic half-space and the wall temperature is $T=1000$ K (solid line) and to $T=1500$ K (dashed line).

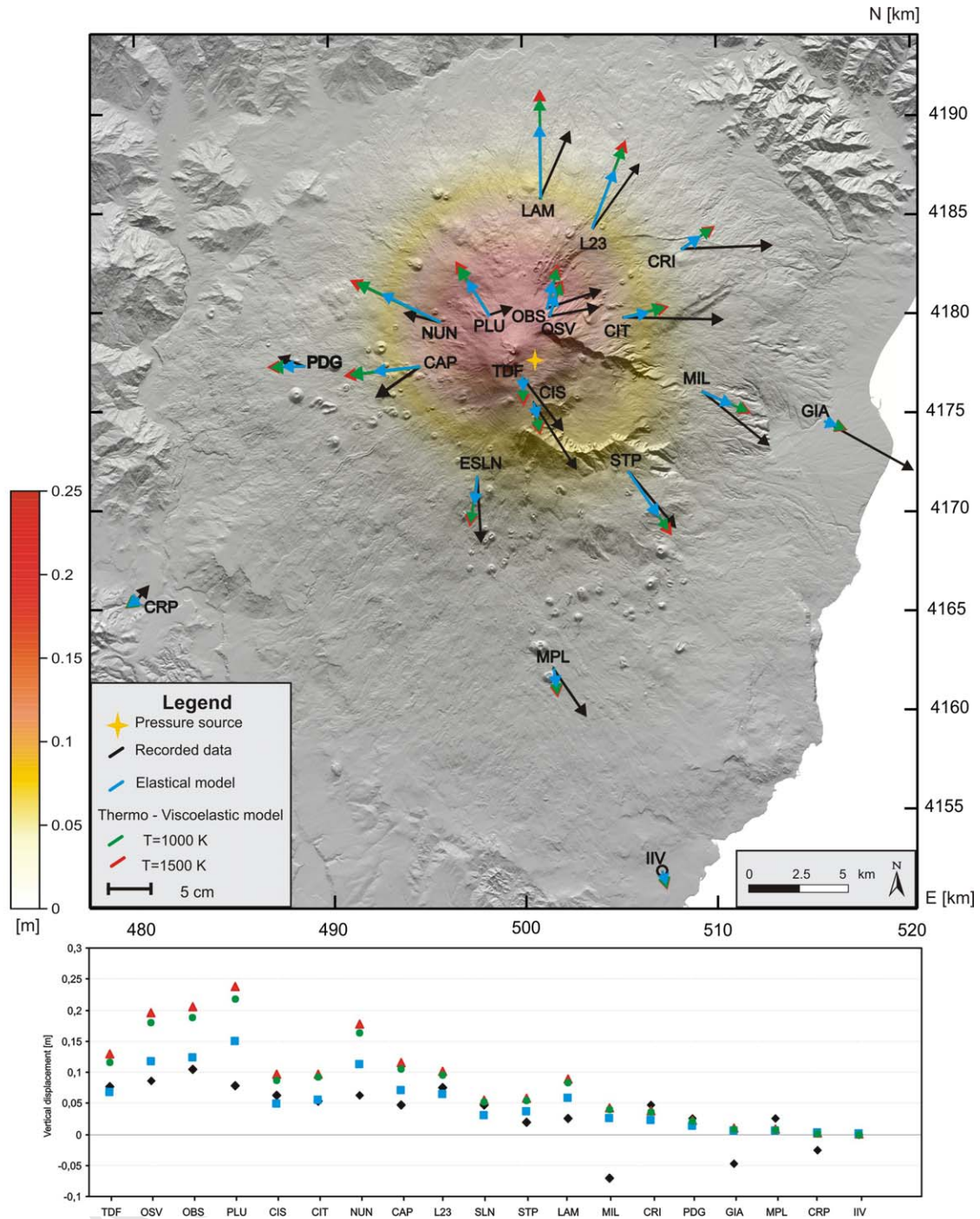


Figure 12 – Comparison between GPS observed (black) and computed deformation during the 1993-1997 period. The numerical computations are performed assuming a heterogeneous elastic medium (blue, after Bonaccorso et al., 2005) and a temperature-dependent viscoelastic medium with pressure source of 320Mpa and source wall temperature at either 1000 K (green) or 1500 K (red).

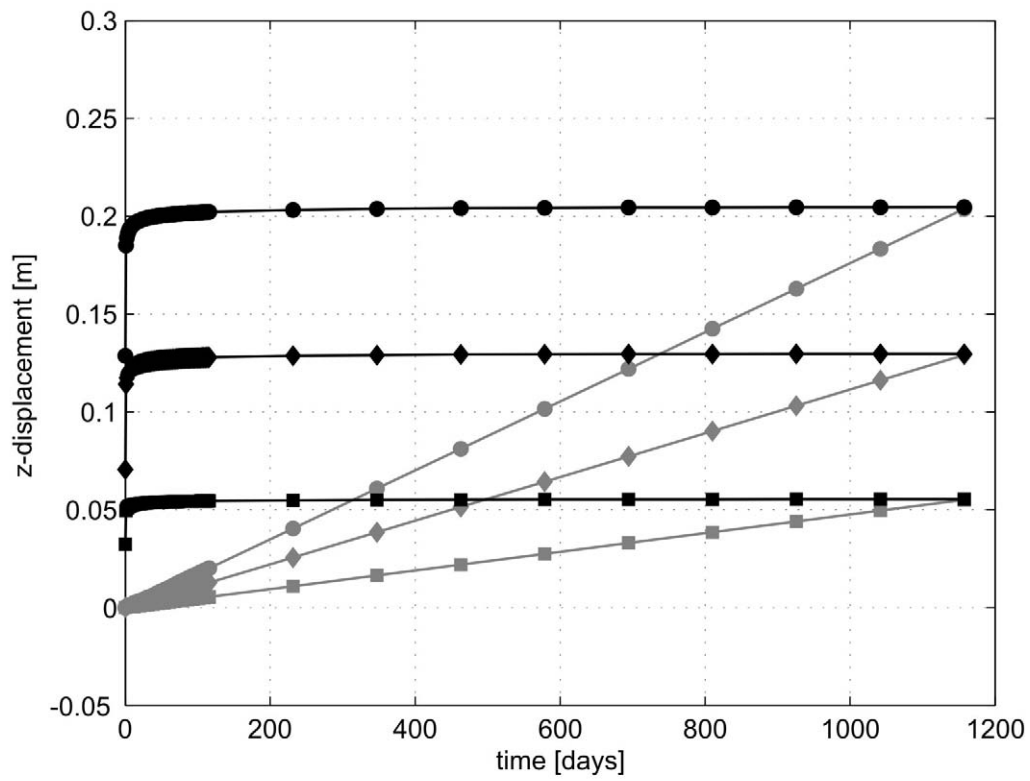


Figure 13 - Vertical uplift at OBS (circle), ESLN (square) and TDF (diamond) computed for a step-like pressure increase (black lines) and linear pressure change (grey lines).